Appl Nanosci (2012) 2:231–238
DOI 10.1007/s13204-012-0095-7

ORIGINAL ARTICLE

Efficacy of highly water-dispersed fabricated nano ZnO against clinically isolated bacterial strains

Shouvik Mitra · Prasun Patra · Sourov Chandra · Panchanan Pramanik · Arunava Goswami

Received: 1 November 2011 / Accepted: 14 March 2012 / Published online: 31 March 2012

Abstract Versatile use of zinc oxide nanoparticles (ZNPs) in semiconductors, optical device and solar cells has already been established. Herein we describe synthesis of surface-functionalized ZNP to highly water dispersible constituent and its antibacterial efficiency against clinically isolated bacterial system. ZNP was synthesized by single-step microwave-assisted route using an aqueous buffer solution. Surface of ZNP was functionalized by grafting of phosphonoacetic acid as the coupling agent. Transmission electron microscopy image suggested that functionalized ZNP was smaller in size in comparison with unfunctionalized one. Antibacterial activity against clinically isolated bacterial strains of *Escherichia coli*, *Staphylococcus aureus* and *Klebseilla* sp. was detected with dose dependency. Functionalized ZNP claimed hexagonal crystal structure and exhibited higher dispersibility in aqueous solution which resulted in the production of greater reactive oxygen species and hence destruction of cell membrane leading to its biocidal efficacy. It is worth mentioning that functionalized dispersed fabricated ZNP would be used as potent biocides in medical as well as agricultural sector.

S. Mitra · P. Patra · A. Goswami (✉)
AERU, Biological Sciences Division, Indian Statistical Institute, Kolkata 700108, India
e-mail: agoswami@isical.ac.in

S. Mitra
e-mail: chemshouvik2009@gmail.com

S. Chandra · P. Pramanik (✉)
Nanomaterials Laboratory, Indian Institute of Technology, Kharagpur 721302, India
e-mail: pramanik1946@gmail.com

S. Chandra
e-mail: chandrasourov@gmail.com

Keywords Nano ZnO · Surface functionalized · Water dispersed · Antibacterial property

Introduction

Nanomedicine is providing unique prospect in development of novel drug as well as drug delivery systems. Therefore, nanotechnology-based biological applications have been hotly pursued in recent times, which involves innumerous metal oxide as the tool. Functionalized nanosilica is effectively used against malaria (Goswami et al. 1996, 1997; Singh et al. 2002) and lethal virus BmNPV (Rahman et al. 2009; Goswami et al. 2009). Amongst the metal oxides zinc oxide has been found to be one of the most potent metal oxides which are rather considered as GRAS (generally recognized as safe) by US food and drug administration (Mitra et al. 2012). Zinc oxide has some advantages; first it is a semiconductor with a band gap of 3.37 eV and large exciton binding energy of 60 meV. Second it is piezoelectric, which is a key property in building electromechanical coupled sensors and transducers. Finally, zinc oxide is biocompatible and can be used without further coating (Wang 2004). Versatile use of zinc oxide nanoparticles (ZNPs) in semiconductors, biosensors (Ren et al. 2009), optical device (Yude et al. 2006) and solar cells (Lee et al. 2008) has already been established; biocidal efficacy of ZNP against some microbial system (Padmavathy and Vijayaraghavan 2008; Reddy et al. 2007) has been proved already while others are in progress.

Unique properties of metal oxide nanoparticles are attributed towards high surface areas with unusual crystal morphologies that possess numerous edge/corner and other reactive surface sites (Klabunde et al. 1996). Though toxicological issues are associated with nanoparticles for

biosafety prospect, nanoscale ZnO of size range 20–100 nm can be employed as a safe nanomaterial as it scatters and reflects UV in sunlight (Huang et al. 2008). Zinc oxide nanoparticles (ZNPs) are believed to be non-toxic and biocompatible (Zhou et al. 2006) and are therefore used in drug carrier and filling in medical materials (Ito 1991). Antibacterial activity of ZnO of size ranging from nanometer to micrometer range has been established by Yamamoto et al. (2008), while Applerot et al. (2009) proposed that reactive oxygen species (ROS) is responsible behind the toxicity. Transition-metal-doped ZnO is effective against *Escherichia coli* as shown by Dutta et al. (2010). Herein, we demonstrate a simple microwave-assisted route for the formation of ZNPs followed by a single-step fabrication to its highly water-dispersible constituents and its efficacy against clinically isolated gram-positive bacterial strains of *E. coli*, *Staphylococcus aureus* and gram-negative bacterial strain of *Klebseilla* sp.

Most of the studies done so far involved direct application of ZNPs or doped ZNPs towards microbial system. The major difficulty arises when these nanoparticles undergo agglomeration; especially ZNPs have a tendency to undergo agglomeration. In the same pursuit, we have tried to minimize the agglomeration tendency via single-step fabrication using phosphonoacetic acid to its highly water-dispersible form. Since ROS is responsible for biocidal toxicity, highly dispersed nanoparticles of ZnO are effective against clinically isolated drug-resistant bacterial system; details biocidal activity are in progress. Hence the main objectives of our studies are (a) microwave-assisted new synthesis of ZNP by our group, (b) single-step fabrication of ZNP to its highly water-dispersed form, (c) dispersed ZnO has small size range in comparison with the native one without altering the crystal structure and (d) dose-dependant efficacy of those fabricated nano ZnO against clinically isolated bacterial strains. Attempts have been made to explain the biocidal efficacy of fabricated nano ZnO.

Materials and methods

Zinc acetate dihydrate, tris(hydroxymethyl)aminomethane (TRIS), Ethanol and Sodium hydroxide were purchased from Merck (India), phosphonoacetic acid was purchased from Sigma Aldrich and Muller Hilton broth was obtained from Himedia. All the chemicals were of analytical grade and used without further purification. Milli-Q grade water (Sartorious Stedim Biotech) was used for biological experiment with conductivity less than 0.1 μS/cm.

Experimental section

Synthesis of zinc oxide nanoparticle (ZNP)

Most of the reported methods involved drastic synthetic route under highly alkaline conditions (Wang et al. 2004) but our process showed a simple pathway at a shorter time. Briefly, to 25 mL of 0.05 M zinc acetate dihydrate solution, 20 mL 20 % aqueous TRIS solution was added drop wise. The mixture was stirred well and then subjected to microwave irradiation at 300 W for 3 min in a domestic microwave. The obtained product was centrifuged at 10,000 rpm for 10 min and washed several times with milli-Q water to remove excess of TRIS buffer. Finally, the product was washed with ethanol and dried overnight at 80 °C in a hot air oven.

Functionalization of zinc oxide nanoparticle by phosphonoacetic acid (ZNPA)

As obtained ZNP of weight 500 mg was allowed to disperse in 50 mL of ethanol in a sonication bath for 30 min. To it 50 mg of phosphonoacetic acid dissolved in 10 mL of water was added drop wise followed by the addition of 1 N NaOH; pH of the reaction mixture was adjusted to 7–8. The reaction mixture was allowed to stir for 6 h when white solid ZnO was precipitated from the reaction mixture. The precipitate was collected and washed several times with ethanol to remove the unreacted phosphonoacetic acid; finally, the product was dispersed in milli-Q water.

Isolation of bacterial strain

Pathogenic bacterial strains of *E. coli*, *Staphylococcus aureus* and *Klebseilla* sp. were isolated from clinical specimens (urine, throat swab and pus) which were grown in Muller Hilton broth medium. All strains were grown aerobically at 37 °C in 10 mL of medium in 18 mm × 150 mm borosilicate glass culture tubes (Borosil) with shaking at 150 rpm under normal laboratory lighting conditions unless otherwise specified.

Antibacterial assay

Bactericidal effect of ZNPA nanoparticles was studied against gram-negative and gram-positive bacteria. These nanoparticles were dispersed in autoclaved deionized water. Aqueous dispersions of ZNPA nanoparticles of desired concentrations were made. An axenic culture of clinically isolated *E. coli, Staphylococcus aureus* and *Klebseilla* sp. was grown in liquid Muller Hilton broth medium. For this experimental investigation, freshly grown

bacterial inoculums (1×10^6 cells/mL) of three bacterial strains were incubated in the presence of a range of ZNPA nanoparticles loadings 1, 2, 5, 10, 20, 40, 60, 80, 160, 320, 500 and 1,000 μg/mL added in each flask along with a control (only media) to observe the bacterial cell growth at 37 °C and 150 rpm. Total solution volume in each glass tube was kept 10 mL. In liquid medium, the growth of bacterial strains was indexed by measuring optical density (OD) at 600 nm against abiotic control using UV–VIS spectrophotometer (Dutta et al. 2010).

Characterization

Morphology was investigated using SUPRA 40 Field Emission Scanning Electron Microscope of Carl Zeiss with acceleration voltage of 5.0 kV. For FESEM alcoholic dispersion of ZNP was put on a properly cleaned glass slide followed by spin coating. UV–VIS spectra of the sample were carried out using Shimadzu absorption spectrophotometer (Model No. 1700), and photoluminescence spectrum was recorded in Hitachi spectrofluorimeter (model no: F-7000). XRD of the sample was carried out in PANalytical X-PERT PRO applying a primary beam monochromator to select the Kα1 component of the employed copper radiation (wavelength of 1.54056 Å). FTIR spectra were recorded in Perkin-Elmer spectrum 100. Prior to FTIR measurements the samples were ground with KBr (spectroscopic grade) and pressed to pellets. Particle size was determined using transmission electron microscopy (TEM) of Phillips CM 200 at an operational voltage of 200 kV. For TEM micrograph a well-dispersed solution of the sample in ethanol was put into uniform carbon-coated copper TEM grid and well dried in vacuum. For antibacterial efficacy OD of the samples were measured using the same UV–VIS spectrometer with determination of MIC and the results were analyzed statistically. Zeta potential of the sample was measured using Malvern zetasizer instrument, and thermal stability was investigated by TG–DTA analysis carried out in Perkin-Elmer (diamond series), with a heating rate of 10 °C/min under nitrogen atmosphere.

Results and discussion

Herein we described successful microwave-assisted chemical synthesis of ZNP followed by surface functionalization with phosphonoacetic acid to its highly water-dispersible form. TRIS buffer was used in the first synthetic step which itself was a standard nontoxic buffer and inert to a wide variety of chemicals and biomolecules and therefore extremely satisfactory for biochemical reactions. TRIS here allowed the reaction at mild experimental condition at the same time allowing the growth of a crystal structure of ZNP with its polydentate nature (Polleux et al. 2005). Synthesis of ZnO nanocrystal or nanorod at low temperature required strong alkaline medium (Wang et al. 2004) but in this process TRIS buffer provided elevated buffer capacity at the same time suitable for biological purposes (Good et al. 1966). Though Bauermann et al. (2006) reported the ZnO nanocrystal in the presence of TRIS buffer, the particles were not well distinct from TEM micrograph and were extremely agglomerated; meanwhile crystalline nature was not quite predominant and high-temperature annealing was required. In that prospect our process is quite easy, cheap and eco-friendly as well.

Particle size distributions (PSD) with hydrodynamic radius of synthesized ZNP and phosphonoacetic acid functionalized zinc oxide nanoparticle (ZNPA) wee recorded from Dynamic Light Scattering using a laser light ($\lambda = 660$ nm) scattered at an angle $\theta = 90°$ at 25°, placing the dispersion in a glass cuvette. A well-diluted ZNP and ZNPA dispersion in milli-Q water was taken in a test tube and sonicated for 30 min in a sonication bath. The average hydrodynamic size distribution was found to be less than 100 nm for ZNPs which was further decreased than the previous one after functionalization in ZNPA (data not shown). When dispersional stability of ZNPA was observed against time (6, 12 and 24 h), remarkably no significant change in hydrodynamic radius was observed which justified that ZNPA dispersions were stable with respect to time (shown in Fig. 1).

UV–VIS property of ZNPs and ZNPA was observed in aqueous dispersion which hinted smaller PSD in functionalized ZNP; Fig. 2 represented the UV–VIS absorbance. ZNPs exhibited a characteristic peak of zinc oxide at 362 nm (Bhattacharyya and Gedanken 2008) which was marginally shifted to 369 nm after surface functionalization. The nature of the peaks was identical but ZNPA produced a sharp peak in comparison with the

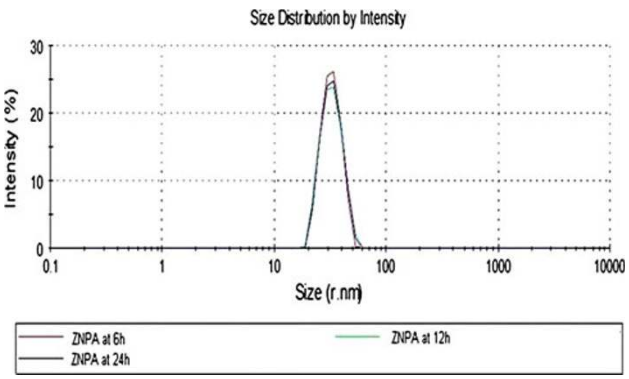

Fig. 1 Measurement of hydrodynamic radius against time as a function of dispersional stability

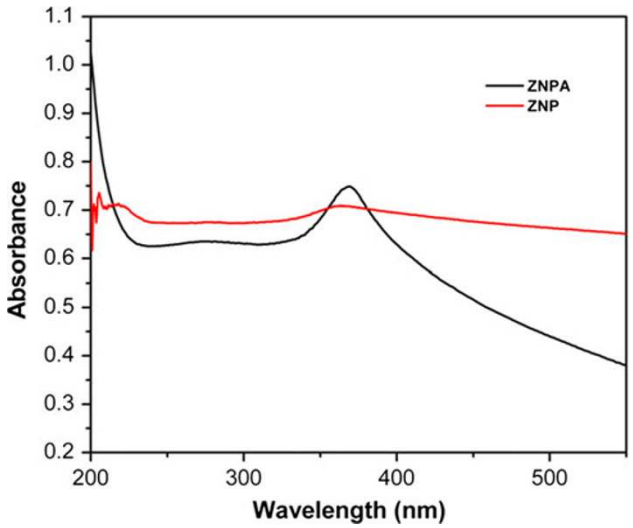

Fig. 2 UV–VIS absorbance of ZNP and ZNPA, respectively

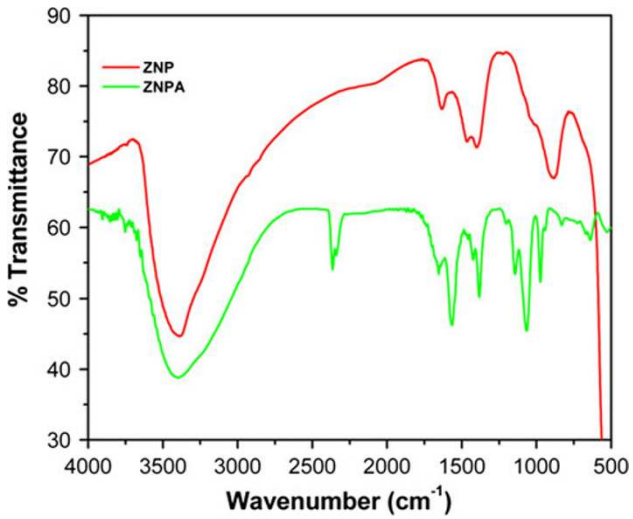

Fig. 3 FTIR spectra of ZNP and ZNPA

unfunctionalized one which justified more dispersed particle in the later one.

Successful surface functionalization was confirmed by FTIR spectra; FTIR spectra of ZNP and ZNPA are represented in Fig. 3. ZNP exhibited five characteristic peaks of which 3,393 cm^{-1} peak signified O–H stretching frequency. Small peaks obtained at 1,633 and 890 cm^{-1} justified C=O (carbonyl) and Zn–O stretching signifying its small amount. The peaks obtained in the region of 1,400 and 1,462 cm^{-1} pertained to O–H and N–H bending though the amount of N–H group was less. After functionalization by phosphonoacetic acid ZNPA exhibited a broad peak at 3,406 cm^{-1} which was signified by the increase in the number of surface O–H group. In post fabricated ZNP, C=O stretching of carboxylic acid was shifted to higher wave number (1,658 cm^{-1}) and 1,568 cm^{-1} indexed the presence of $-CO_2^-$ asymmetric stretching of carboxylic acid as reported by Zhang et al. (2010), while P=O stretching frequency was observed within 1,149–1,209 cm^{-1} and O–H, N–H bending was observed at 1,431, 1,384 cm^{-1}, respectively. In our study, $-CO_2^-$ band was more intense as we carried out the reaction in mild alkaline condition which allowed the carboxylic acid group to undergo its deprotonation.

Powder XRD of nano ZnO exhibited ten characteristic peaks with $2\theta = 31.55°$, 34.16°, 35.99°, 47.19°, 56.33°, 62.46°, 66.22°, 67.68°, 68.83° and 76.67° which could easily be indexed to (100), (002), (101), (102), (110), (103), (200), (112), (201) and (202) diffraction planes with hexagonal structure (JCPDS card no. 034477) (Sharma et al. 2010). After functionalization by phosphonoacetic acid the peak positions were almost unshifted with $2\theta = 31.79°$, 34.41°, 36.24°, 47.59°, 56.58°, 62.83°, 66.37°, 67.93°, 69.11° and 76.92° which were also justified to (100), (002), (101), (102), (110), (103), (200), (112), (201) and (202) diffraction planes of ZnO. XRD diffraction pattern was depicted in Fig. 4; no additional peaks were obtained in the diffraction pattern which encountered its chemical purity. These two figures indexed that the crystalline structure was inherently unchanged after functionalization.

ZNPs were nearly spherical in nature as revealed from FESEM micrograph. Figure 5a represented FESEM micrograph of ZNPs and Fig. 5b showed the corresponding EDX spectrum which justified that Zn and O were the main chemical constituents. Two additional peaks were obtained which corresponded to Si and Au coming from spin coating of the sample present in a glass slide. However, accurate size of ZNP and ZNPA was determined by TEM analysis. The most splendid observation of our experiment was reduction in size after functionalization by phosphonoacetic acid. Initial size range of ZNP was around 18–20 nm which was reduced to 12–14 nm after functionalization which delivered more dispersity of the ZNPA nanoparticles. Figure 6a and b showed the TEM image of ZNP and ZNPA, respectively. Before functionalization the particles were more agglomerated but after functionalization spherical distinct particles were obtained. SAED pattern of ZNP and ZNPA reflected their crystalline structure which was shown in Fig. 6a and b inset, respectively.

ZNP was found to be stable up to temperature range of 700 °C while ZNPA underwent weight loss from low to higher temperature range. For ZNP only 0.7 % weight loss was observed at 100 °C which was due to subsequent loss of water molecules; a total 2.84 % of weight loss up to 700 °C was attributed towards dead sorption of the bound water molecules. On the other hand, ZNPA showed 3.7 % of weight loss at 100 °C which can be explained by loss of water molecules from its surface and a total of 20.41 %

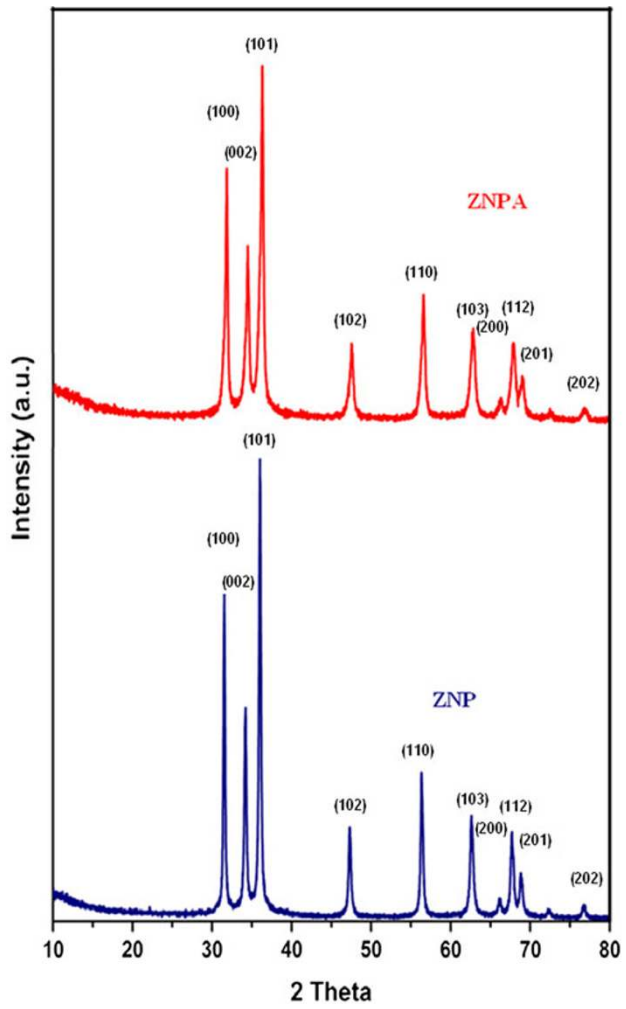

Fig. 4 XRD pattern of ZNP and ZNPA, respectively

weight loss was observed throughout the temperature range of 700 °C. Weight loss above 100 °C was justified by the loss of water adsorbed and the rupture of the organic fragment phosphonoacetic acid at high temperature above its melting point of 145 °C and boiling point of 490 °C along with decarboxylation from CO_2H fragment. A plot of percentage weight loss against temperature was shown in Fig. 7a. The small size of ZNPA and its highly dispersed nature were reflected in zeta potential and photoluminescence (PL) property. ZNPs have zeta potential value of about −11.5 mV at pH 8 which was increased to −23.2 mV at same pH for ZNPA justifying its smaller size distribution and higher dispersibility. Figure 7b showed the PL property of ZNPs and ZNPA, respectively. Two-peak PL curve was obtained when it was excited at 340 nm. The emission band was centered 380 and 419–438 nm, but ZNPA possessed higher intense emission band and marginal splitting was observed in the broad emission band which was suppressed in ZNP. This could be due to the smaller size distribution and higher water dispersed nature of ZNPA in comparison with ZNP. Among the two bands, the lower was attributed to the recombination of excitons (Vanheusden et al. 1996) while the broad peak could be indexed to singly ionized oxygen vacancy in ZnO.

ZNPA showed a significant growth inhibition compared with the control against all three drug-resistant bacterial strains. The dynamics of bacterial growth were monitored after 24 h of inoculums of bacteria by measuring the OD (at 600 nm) of the control, and bacterial solutions supplemented with different concentration of ZNPA are shown in Fig. 8. Bacterial cell growth enhanced the turbidity of the liquid medium and as a result absorbance was increased.

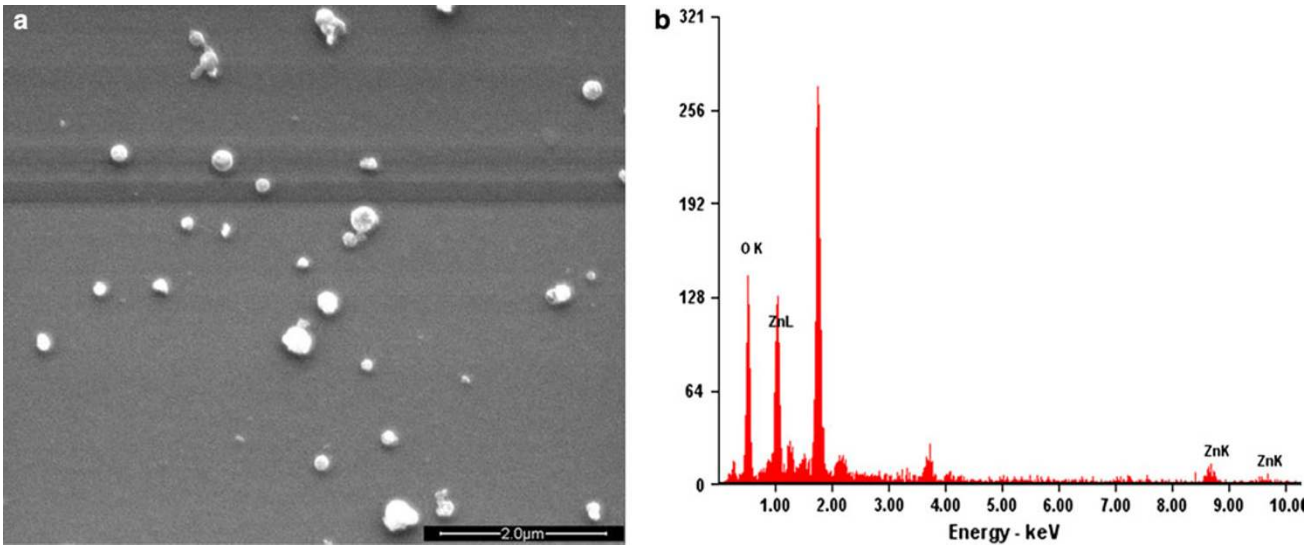

Fig. 5 **a** FESEM image of ZNP, **b** EDX spectrum of ZNP illustrating its chemical composition

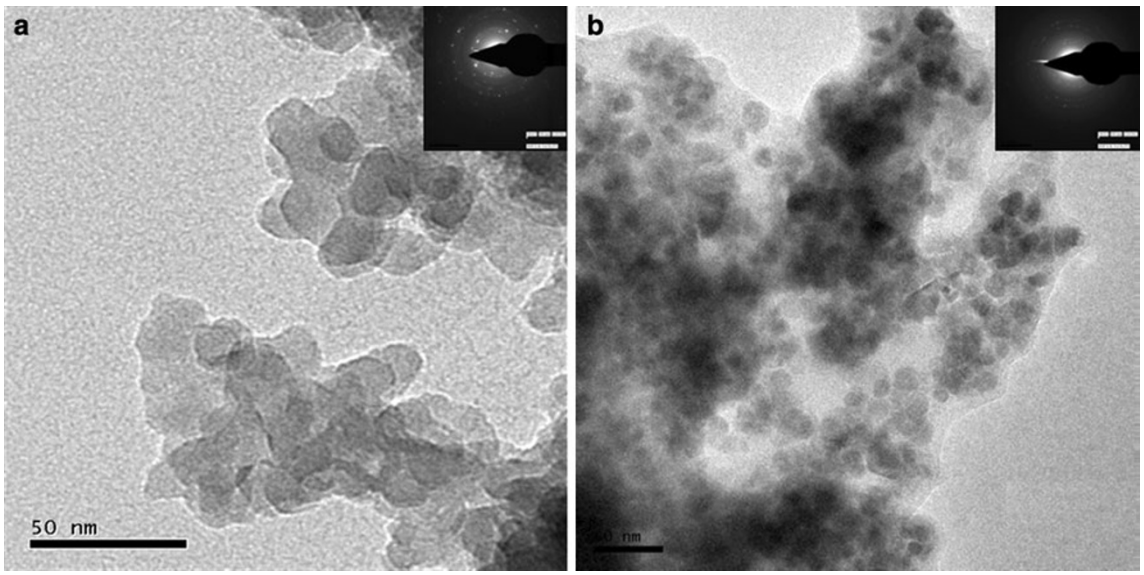

Fig. 6 **a** TEM image of ZNP with *inset* indicating SAED pattern of the same, **b** TEM image of ZNPA with *inset* illustrating the SAED pattern of ZNPA

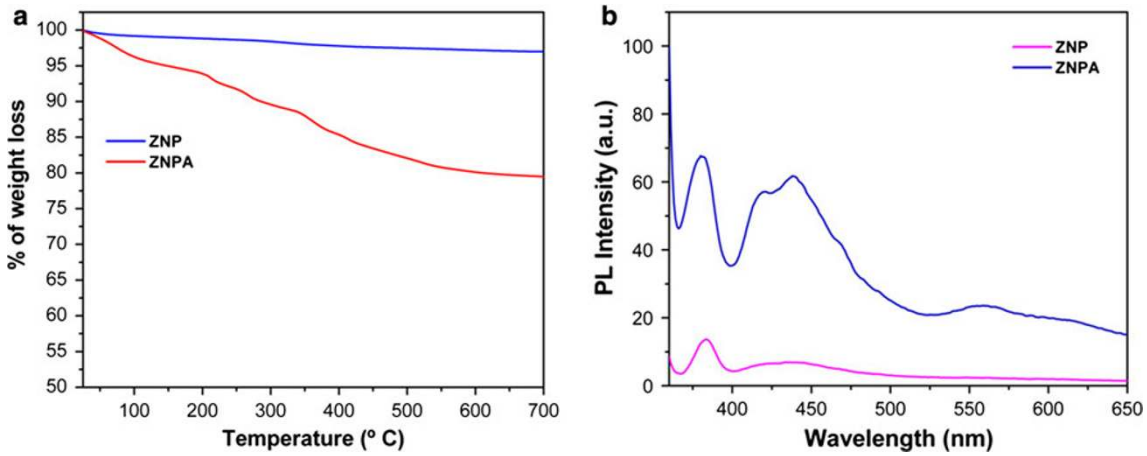

Fig. 7 **a** Thermo gravimetric plot of percentage weight loss against temperature of ZNP and ZNPA, respectively, **b** PL spectra of ZNP and ZNPA, respectively

It was clear that at all these concentrations, the nanoparticles caused a growth delay of the bacterial cells; slope of the bacterial growth curve continuously decreased with increasing ZNPA concentration. Minimum inhibitory concentration (MIC) was determined at which no bacterial growth was visible (Mitra et al. 2012); for clinically isolated bacterial strains MIC was determined after 24 h of inoculums (Pfaller et al. 2011). ZNPA of highest concentration 40 μg/mL showed no growth after 24 h of inoculums which was found to be the MIC value. Enhanced bioactivity of ZNPA was observed by studying the antimicrobial activity of suspensions using a standard microbial method for the first time. Antibacterial effect of ZNP was previously studied, but common ZNPs were partially water dispersed and underwent agglomeration as observed from TEM image (Bauermann et al. 2006). Small-sized and dispersed NPs could contribute to higher cellular uptake. Therefore, more dispersed and small-sized particle would be beneficial in antibacterial assay; ZNPA was fully water dispersed and particles were fully dispersed in broth medium which resulted in the generation of a larger number of active oxygen species (released from ZNPA on to the surface of the bacterial suspension) more effectively. Hence ZNPA contributed to the greater mechanical damage of the cell membrane by generating ROS after adhesion of ZNPA on to the bacterial cell surface, similar to the report of adhesion of ZNPs by Jiang et al. (2010).

The effectiveness of zinc oxide-based compounds was attributed to its photocatalytic property using which free electrons and holes could be generated by light, stronger

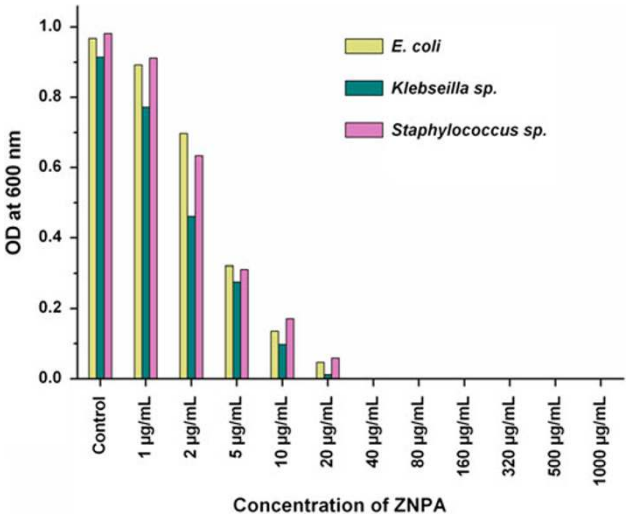

Fig. 8 Determination of MIC value of ZNPA against clinically isolated strains of *Escherichia coli*, *Staphylococcus aureus* and *Klebseilla* sp.

than its band gap energy. These electron–hole pairs diffuse out to the surface and transform the surrounding oxygen or water molecules into hydroxyl radicals as the holes are strong oxidant (Jang et al. 2006; Yin and Casey 2010). These were in fact the reasons for the generation of fatal ROS. More smaller and dispersed particles were expected to produce higher ROS in aqueous medium which was again followed up by ZNPA with its higher dispersibility. FTIR spectra signified the presence of $-CO_2^-$ band and higher negative zeta potential also justified their presence which allowed the particles to be more dispersed in aqueous solution; therefore, ZNPA was capable of producing greater ROS in comparison with ZNPs. ZNPA retrieve hexagonal crystal structure with (101) plane the highest intense indicating their possible growth along [0001] direction as reported by Huang et al. (2008) which was again important towards the cytotoxicity and biocidal efficacy.

Conclusion

In conclusion, we have reported a simple technique to fabricate ZNPs to its highly water-dispersed form. ZNPs were synthesized by a microwave-assisted process with the help of a buffer which was nontoxic to wide variety of biological systems and hence applicable in physiological conditions. Post fabricated ZNPs infatuated smaller size distribution of particles; FTIR and zeta potential justified higher dispersibility of the particles. Antibacterial activity against clinically isolated bacterial strains of *E. coli*, *Staphylococcus aureus* and *Klebseilla* sp. was calibrated. Dose-dependant efficacy was observed with 40 µg/mL ZNPA, the benchmark concentration during the evaluation of MIC. ZNPA was fully water dispersed and particles were able to produce a homogeneous dispersion over the bacterial suspension in the medium which resulted in the generation of a larger number of active oxygen species on to the surface of the bacterial suspension more effectively resulting in cell membrane destruction and removal of cytoplasmic contents. Crystalline structure was unchanged after functionalization allowing them to grow along [0001] direction which was significant towards biocidal efficacy. It is worth mentioning that functionalized dispersed ZNPA could be used as potent biocides in medical as well as agricultural sector.

Acknowledgments The authors would like to thank Department of Biotechnology, Govt. of India (DBT) (grant no. BT/PR9050/NNT/28/21/2007 and BT/PR8931/NNT/28/07/2007) and NAIP for their generous financial support. SM is thankful to CSIR for their financial support and ISI plan project 2008–2011 for funding this work and collaborative efforts.

References

Applerot BG, Lipovsk A, Dror R, Perkas N, Nitzan Y, Lubart R, Gedanken A (2009) Enhanced antibacterial activity of nanocrystalline ZnO due to increased ROS-mediated cell injury. Adv Funct Mater 19(6):842–852

Bauermann LP, Bill J, Aldinger F (2006) Bio-friendly synthesis of ZnO nanoparticles in aqueous solution at near-neutral pH and low temperature. J Phys Chem B 110:5182–5185

Bhattacharyya S, Gedanken A (2008) A template-free, sonochemical route to porous ZnO nano-disks. Microporous Mesoporous Mater 110:553–559

Dutta RK, Sharma PK, Bhargava R, Kumar N, Pandey AC (2010) Differential susceptibility of Escherichia coli cells toward transition metal-doped and matrix-embedded ZnO nanoparticles. J Phys Chem B 114:5594–5599

Good NE, Winget GD, Winter W, Connolly TN, Izawa S, Singh RM (1966) Hydrogen ion buffers for biological research. Biochemistry 5(2):467–477

Goswami A, Chatterjee S, Sharma S (1996) Cloning of a ribosomal phosphoprotein P0 gene homologue from *Plasmodium falciparum*. Mol Biochem Parasitol 82(1):117–120

Goswami A, Singh S, Redkar VD, Sharma S (1997) Characterization of P0, a ribosomal phosphoprotein of *Plasmodium falciparum* antibody against amino-terminal domain inhibits parasite growth. J Biol Chem 272(18):12138–12143

Goswami A, Rahman A, Biswas N, Ulrichs C, Buttner C, Bramhachary RL, Datta A (2009) Nanoparticle–virus complex shows enhanced immunological effect against baculovirus. J Nanosci Nanotechnol 9:1–5

Huang Z, Zheng X, Yan D, Yin G, Liao X, Kang Y, Yao Y, Huang D, Hao B (2008) Toxicological effect of ZnO nanoparticles based on bacteria. Langmuir 24:4140–4144

Ito M (1991) In vitro properties of a chitosan-bonded hydroxyapatite bone-filling paste. Biomaterials 12(1):41–45

Jang YJ, Simer C, Ohm T (2006) Comparison of zinc oxide nanoparticles and its nano-crystalline particles on the photocatalytic degradation of methylene blue. Mater Res Bull 41(1):67–77

Jiang W, Yang K, Vachet RW, Xing B (2010) Interaction between oxide nanoparticles and biomolecules of the bacterial cell envelope as examined by infrared spectroscopy. Langmuir 26(23):18071–18077

Klabunde KJ, Stark J, Koper O, Mohs C, Park D, Decker S, Jiang Y, Lagadic I, Zhang DJ (1996) Nanocrystals as stoichiometric reagents with unique surface chemistry. Phys Chem 100(30): 12142–12153

Lee YJ, Ruby DS, Peters DW, McKenzie BB, Hsu JWP (2008) ZnO nanostructures as efficient antireflection layers in solar cells. Nano Lett 8(5):1501–1505

Mitra S, Chandra S, Laha D, Patra P, Debnath N, Pramanik A, Pramanik P, Goswami A (2012) Unique chemical grafting of carbon nanoparticle on fabricated ZnO nanorod: antibacterial and bioimaging property. Mater Res Bull 47:586–594

Padmavathy N, Vijayaraghavan R (2008) Enhanced bioactivity of ZnO nanoparticles—an antimicrobial study. Sci Technol Adv Mater 9:035004–035010

Pfaller MA, Boyken L, Hollis RJ, Kroeger J, Messer SA, Tendolkar S, Diekema DJ (2011) Wild-type MIC distributions and epidemiological cutoff values for posaconazole and voriconazole and *Candida* spp. as determined by 24-hour CLSI broth microdilution. J Clin Microbiol 49(2):630–637

Polleux J, Pinna N, Antonietti M, Hess C, Wild U, Schlogl R, Niederberger M (2005) Ligand functionality as a versatile tool to control the assembly behavior of preformed titania nanocrystals. Chem Eur J 11:3541–3551

Rahman A, Seth D, Mukhopadhyaya SK, Brahmachary RL, Ulrichs C, Goswami A (2009) Surface functionalized amorphous nanosilica and microsilica with nanopores as promising tools in biomedicine. Naturwissenschaften 96:31–38

Reddy KM, Feris K, Bell J, Wingett DG, Hanley C, Punnoose A (2007) Selective toxicity of zinc oxide nanoparticles to prokaryotic and eukaryotic systems. Appl Phys Lett 90:213902-1–213902-3

Ren X, Chen D, Meng X, Tang F, Hou X, Han D, Zhang L (2009) Zinc oxide nanoparticles/glucose oxidase photoelectrochemical system for the fabrication of biosensor. J Colloid Interface Sci 334(2):183–187

Sharma D, Rajput J, Kaith BS, Kaur M, Sharma S (2010) Synthesis of ZnO nanoparticles and study of their antibacterial and antifungal properties. Thin Solid Films 519(3):1224–1229

Singh S, Sehgal A, Goswami A, Waghmare S, Chakrabarty T, Sharma S (2002) Surface expression of the conserved ribosomal protein P0 on parasite and other cells. Mol Biochem Parasitol 119(1): 121–124

Vanheusden K, Warren V, Seager CH, Tallant DR, Voigt JA, Gnade BE (1996) Mechanism behind green photoluminescence in ZnO phosphor powders. J Appl Phys 79:7983–7990

Wang ZL (2004) Nanostructures of zinc oxides. Mater Today 7(6): 26–33

Wang Z, Qian XF, Yin J, Zhu ZK (2004) Large-scale fabrication of tower-like, flower-like and tube-like ZnO arrays by a simple chemical solution route. Langmuir 20:3441–3448

Yamamoto O, Komatsu M, Sawai J, Nakagawa Z (2008) Antibacterial activity of ZnO powder with crystallographic orientation. J Mater Sci Mater Med 19(3):1407–1412

Yin H, Casey PS (2010) Effects of surface chemistry on cytotoxicity, genotoxicity and the generation of reactive oxygen species induced by ZnO nanoparticles. Langmuir 26(19):15399–15408

Yude W, Shuo Z, Xinghui W, Qingju L (2006) Synthesis and optical properties of nano-ZnO particles/mesostructured SnO_2 composite. Mater Chem Phys 98(1):121–124

Zhang B, Kong T, Xu W, Su R, Gao Y, Cheng G (2010) Surface functionalization of zinc oxide by carboxyalkylphosphonic acid self-assembled monolayers. Langmuir 26(6):4514–4522

Zhou J, Xu NS, Wang ZL (2006) Dissolving behavior and stability of ZnO wires in biofluids: a study on biodegradability and biocompatibility of ZnO nanostructures. Adv Mater 18:2432–2435